XL CILAMCE
IBERO-LATIN AMERICAN CONGRESS ON COMPUTATIONAL METHODS IN ENGINEERING
NOVEMBER 11-14, 2019
Praiamar Natal Hotel & Convention
Natal, RN-BRAZIL

PHYSICAL REFLECTIVE BOUNDARY CONDITIONS APPLIED TO SMOOTHED PARTICLE HYDRODYNAMICS METHOD FOR SOLVING THREE-DIMENSIONAL FLUID DYNAMICS PROBLEMS

Carlos Alberto Dutra Fraga Filho[1,2*]

Chong Peng[1]

Md Rushdie Ibne Islam[1]

Christopher McCabe[1]

Samiullah Baig[1]

Gonella Venkata Durga Prasad[1]

[1] ESS Engineering Software GmbH - Berggasse 35, 4400, Steyr, Austria

[2] Development, Implementation and Application of Computational Tools for Problem Solving in Engineering Research Group Federal Institute of Education, Science and Technology of Espírito Santo - Av. Vitória, 1729, 29040-780, Jucutuquara, Vitória–ES, Brazil

Correspondent author's email: cadff1@gmail.com

Abstract. The mixing of continuum and microscopic laws is a contradiction often existing in the boundary conditions utilised in meshfree particle methods. Boundary techniques employing fictitious (or ghost) particles and artificial forces (defined in the molecular microscopic scale) are still used in SPH simulations and should be avoided. Currently, there is an effort in replacing boundary techniques that mix concepts of different scales by others that respect the continuum laws. This paper aims to present the implementation of the physical reflective boundary conditions (RBC) in Smoothed Particle Hydrodynamics (SPH) method for solving three dimensional (3-D) fluid dynamics problems. In this work, SPH was applied to solve the physical conservation equations for a Newtonian, incompressible, uniform and isothermal fluid. Applications in hydrostatics and hydrodynamics are presented as well as the validation of the results in 3-D domains. Two problems were studied: a still fluid inside an immobile reservoir and dam breaking flow. The results achieved presented a good agreement with the analytical solution and literature data.

Keywords: Smoothed Particle Hydrodynamics, reflective boundary conditions, fluid dynamics, continuum mechanics.

Notation

C_o initial position of the centre of mass of the particle (initial instant of the numerical iteration)

$(C_o)_k$ coordinates of the initial position of the centre of mass

C_l position of the centre of mass, in a motion without obstacles, at the end of the numerical iteration

$(C_l)_k$ coordinates of the centre of mass position, in a motion without obstacles, at the end of the numerical iteration

$(C_1)_N$ coordinates of the centre of mass normal to the collision plane, in a motion without obstacles, at the end of the numerical iteration

C_f position of the centre of mass obtained after the collision response

$(C_f)_k$ coordinates of the centre of mass position, after the collision response

$(C_f)_N$ coordinates of the centre of mass position, normal to the collision plane, after the collision response

CR coefficient of restitution of kinetic energy

CF coefficient of friction

g gravity

g gravity magnitude

h support radius

H vertical coordinate of the free surface in the reservoir

k Cartesian direction

m_b mass of the neighbouring particle

P_a absolute pressure acting on the fixed particle

P_b absolute pressure acting on the neighbouring particle

P_{mod} modified pressure

$P_{\text{mod}(a)}$ modified pressure of the fixed particle

$P_{\text{mod}(b)}$ modified pressure of the neighbouring particle

P_0 pressure of reference

t time

v fluid velocity

$\mathbf{v}_a$ velocity of the reference particle

$\mathbf{v}_b$ velocity of the neighbouring particle

$\mathbf{v}_{ab}$ relative velocity between a fixed and a neighbouring particle

V_{ok} component of the initial velocity of the particle (initial instant of the numerical iteration)

V_{fk} component of the final velocity of the particle (final instant of the numerical iteration)

W kernel or interpolation function

$\boldsymbol{X}_a$ position of the reference particle

$\boldsymbol{X}_b$ position of the neighbouring particle

z vertical coordinate of the fluid inside the reservoir

α_π coefficient used in the calculation of the artificial viscosity

β_π coefficient used in the calculation of the artificial viscosity

Δp parameter used in the calculation of the artificial pressure

$\in$ parameter used in the calculation of the artificial pressure

υ kinematic viscosity of the fluid

ρ density of the fluid

ρ_a density of the reference particle

ρ_b density of the neighbouring particle

υ_a kinematic viscosity of the reference particle

∇ mathematical vector operator nabla

1 Introduction

Recent publications ([1-5]) have been realised aiming to propose new boundary conditions techniques excluding the use of fictitious particles on or adjacent to the contours in meshfree particle methods. Literature [2] presented the first implementation of the RBC, based on Newton's restitution law and foundations of analytic geometry, in two-dimensional (2-D) domains. This paper extends the implementation of the RBC to a higher (3-D) dimension with validation tests and simulation results in both hydrostatics and hydrodynamics cases.

A collision detection and response algorithm has been implemented. Two coefficients were used in the collisions treatment: the kinetic energy restitution coefficient (CR), related to the energy loss in the direction normal to the collision plane, and the friction coefficient (CF), that measures the slow down in the particle's motion parallel to the collision plane. A complete description of the implementation of the algorithm (considering only the effects of the elastic restitution of energy) is in [2]. Literature [1] presents the improvement of the algorithm with the implementation of friction effects.

The remainder of this paper is organised in sections as follows. In Section 2, results of the collision detection and response algorithm are presented. Section 3 brings the cases studies and their numerical results and discussions. Finally, conclusions are in Section 4.

2. Algorithm Validation

Analytical results have been employed to verify the positions and velocities that particles reached after the collisions treatment, at the end of each timestep. The velocity of the particle was considered constant in each step of time and its centre of mass moved linearly along the direction of the velocity from C_o to C_1 (considering a motion without obstacles).

The collisions of one particle against the planes have been verified by the comparison of the final positions and velocities of their centres of mass, provided by the algorithm implemented at the end of each time step, and those obtained from the physical-mathematical modelling (analytical results).

Tests have been carried out, in which the particle radius was 0.01 m. The 3-D closed box had sides of 0.50 m. The time step was 0.25s. The coefficients of restitution of kinetic energy (CR) and friction (CF) received different values. Some tests results achieved are presented in Tables I - IX and Figs. 1 - 9.

Test I: Initial position of the centre of mass: C_o = (0.25, 0.25, 0.25) m; Initial velocity: V_o = (1.00, 0.00, 0.00) m/s; CR = 1.00; CF = 0.00 (see simulation results in Table I and Fig. 1).

TABLE I. Results of the 1st validation test* (SI units).

t**	Input data									Output data					
	V_{ox}	V_{oy}	V_{oz}	C_{ox}	C_{oy}	C_{oz}	C_{1x}	C_{1y}	C_{1z}	C_{fx}	C_{fy}	C_{fz}	V_{fx}	V_{fy}	V_{fz}
0.25	1.00	0.00	0.00	0.25	0.25	0.25	0.50	0.25	0.25	0.48	0.25	0.25	-1.00	0.00	0.00
0.50	-1.00	0.00	0.00	0.48	0.25	0.25	0.23	0.25	0.25	0.23	0.25	0.25	-1.00	0.00	0.00
0.75	-1.00	0.00	0.00	0.23	0.25	0.25	-0.02	0.25	0.25	0.04	0.25	0.25	1.00	0.00	0.00
1.00	1.00	0.00	0.00	0.04	0.25	0.25	0.29	0.25	0.25	0.29	0.25	0.25	1.00	0.00	0.00
1.25	1.00	0.00	0.00	0.29	0.25	0.25	0.54	0.25	0.25	0.44	0.25	0.25	-1.00	0.00	0.00

*Rounded to two decimal places
**Number of collisions in every timestep: 1st - 01; 2nd - 0; 3rd - 01; 4th - 0; 5th - 01

Test II: Initial position of the centre of mass: C_o = (0.25, 0.25, 0.25) m; Initial velocity: V_o = (0.00, 1.00, 0.00) m/s; CR = 1.00; CF = 0.00 (see simulation results in Table II and Fig. 2).

TABLE II. Results of the 2nd validation test* (SI units).

t**	Input data									Output data					
	V_{ox}	V_{oy}	V_{oz}	C_{ox}	C_{oy}	C_{oz}	C_{1x}	C_{1y}	C_{1z}	C_{fx}	C_{fy}	C_{fz}	V_{fx}	V_{fy}	V_{fz}
0.25	0.00	1.00	0.00	0.25	0.25	0.25	0.25	0.50	0.25	0.25	0.48	0.25	0.00	-1.00	0.00
0.50	0.00	-1.00	0.00	0.25	0.48	0.25	0.25	0.23	0.25	0.25	0.23	0.25	0.00	-1.00	0.00
0.75	0.00	-1.00	0.00	0.25	0.23	0.25	0.25	-0.02	0.25	0.25	0.04	0.25	0.00	1.00	0.00
1.00	0.00	1.00	0.00	0.25	0.04	0.25	0.25	0.29	0.25	0.25	0.29	0.25	0.00	1.00	0.00
1.25	0.00	1.00	0.00	0.25	0.29	0.25	0.25	0.54	0.25	0.25	0.44	0.25	0.00	-1.00	0.00

*Rounded to two decimal places
**Number of collisions in every timestep: 1st - 01; 2nd - 0; 3rd - 01; 4th - 0; 5th - 01

Test III: Initial position of the centre of mass: C_o = (0.01, 0.01, 0.01) m; Initial velocity: V_o = (1.00, 1.00, 1.00) m/s; CR = 1.00; CF = 0.00 (see simulation results in Table III and Fig. 3).

TABLE III. Results of the 3th validation test* (SI units).

t**	Input data									Output data					
	V_{ox}	V_{oy}	V_{oz}	C_{ox}	C_{oy}	C_{oz}	C_{1x}	C_{1y}	C_{1z}	C_{fx}	C_{fy}	C_{fz}	V_{fx}	V_{fy}	V_{fz}
0.25	1.00	1.00	1.00	0.01	0.01	0.01	0.26	0.26	0.26	0.26	0.26	0.26	1.00	1.00	1.00
0.50	1.00	1.00	1.00	0.26	0.26	0.26	0.51	0.51	0.51	0.47	0.47	0.47	-1.00	-1.00	-1.00
0.75	-1.00	-1.00	-1.00	0.47	0.47	0.47	0.22	0.22	0.22	0.22	0.22	0.22	-1.00	-1.00	-1.00
1.00	-1.00	-1.00	-1.00	0.22	0.22	0.22	-0.03	-0.03	-0.03	0.05	0.05	0.05	1.00	1.00	1.00
1.25	1.00	1.00	1.00	0.05	0.05	0.05	0.30	0.30	0.30	0.30	0.30	0.30	1.00	1.00	1.00

*Rounded to two decimal places
**Number of collisions in every timestep: 1st - 0; 2nd - 01; 3rd - 0; 4th - 01; 5th - 0

Test IV: Initial position of the centre of mass: C_o = (0.01, 0.01, 0.01) m; Initial velocity: V_o = (1.00, 1.00, 0.00) m/s; CR = 1.00; CF = 0.00 (see simulation results in Table IV and Fig. 4).

TABLE IV. Results of the 4th validation test* (SI units).

t**	Input data									Output data					
	V_{ox}	V_{oy}	V_{oz}	C_{ox}	C_{oy}	C_{oz}	C_{1x}	C_{1y}	C_{1z}	C_{fx}	C_{fy}	C_{fz}	V_{fx}	V_{fy}	V_{fz}
0.25	1.00	1.00	0.00	0.01	0.01	0.01	0.26	0.26	0.01	0.26	0.26	0.01	1.00	1.00	0.00
0.50	1.00	1.00	0.00	0.26	0.26	0.01	0.51	0.51	0.01	0.47	0.47	0.01	-1.00	-1.00	0.00
0.75	-1.00	-1.00	0.00	0.47	0.47	0.01	0.22	0.22	0.01	0.22	0.22	0.01	-1.00	-1.00	0.00
1.00	-1.00	-1.00	0.00	0.22	0.22	0.01	-0.03	-0.03	0.01	0.05	0.05	0.01	1.00	1.00	0.00
1.25	1.00	1.00	0.00	0.05	0.05	0.01	0.30	0.30	0.01	0.30	0.30	0.01	1.00	1.00	0.00

*Rounded to two decimal places
**Number of collisions in every timestep: 1st - 0; 2nd - 01; 3rd - 0; 4th - 01; 5th - 0

Test V: Initial position of the centre of mass: C_o = (0.49, 0.49, 0.49) m; Initial velocity: V_o = (-1.00, -1.00, -1.00) m/s; CR = 1.00; CF = 0.00 (see simulation results in Table V and Fig. 5).

TABLE V. Results of the 5th validation test* (SI units).

t**	Input data									Output data					
	V_{ox}	V_{oy}	V_{oz}	C_{ox}	C_{oy}	C_{oz}	C_{1x}	C_{1y}	C_{1z}	C_{fx}	C_{fy}	C_{fz}	V_{fx}	V_{fy}	V_{fz}
0.25	-1.00	-1.00	-1.00	0.49	0.49	0.49	0.24	0.24	0.24	0.24	0.24	0.24	-1.00	-1.00	-1.00
0.50	-1.00	-1.00	-1.00	0.24	0.24	0.24	-0.01	-0.01	-0.01	0.03	0.03	0.03	1.00	1.00	1.00
0.75	1.00	1.00	1.00	0.03	0.03	0.03	0.28	0.28	0.28	0.28	0.28	0.28	1.00	1.00	1.00
1.00	1.00	1.00	1.00	0.28	0.28	0.28	0.53	0.53	0.53	0.45	0.45	0.45	-1.00	-1.00	-1.00
1.25	-1.00	-1.00	-1.00	0.45	0.45	0.45	0.20	0.20	0.20	0.20	0.20	0.20	-1.00	-1.00	-1.00

*Rounded to two decimal places
**Number of collisions in every timestep: 1st - 0; 2nd - 01; 3rd - 0; 4th - 01; 5th - 0

Test VI: Initial position of the centre of mass: C_o = (0.01, 0.01, 0.01) m; Initial velocity: V_o = (1.50, 1.00, 1.00) m/s; CR = 1.00; CF = 0.10 (see simulation results in Table VI and Fig. 6).

TABLE VI. Results of the 6th validation test* (SI units).

t**	Input data									Output data					
	V_{ox}	V_{oy}	V_{oz}	C_{ox}	C_{oy}	C_{oz}	C_{1x}	C_{1y}	C_{1z}	C_{fx}	C_{fy}	C_{fz}	V_{fx}	V_{fy}	V_{fz}
0.25	1.50	1.00	1.00	0.01	0.01	0.01	0.39	0.26	0.26	0.39	0.26	0.26	1.50	1.00	1.00
0.50	1.50	1.00	1.00	0.39	0.26	0.26	0.76	0.51	0.51	0.22	0.47	0.47	-1.22	-0.81	-0.81
0.75	-1.22	-0.81	-0.81	0.22	0.47	0.47	-0.08	0.27	0.27	0.10	0.27	0.27	1.22	-0.73	-0.73
1.00	1.22	-0.73	-0.73	0.10	0.27	0.27	0.41	0.09	0.09	0.41	0.09	0.09	1.22	-0.73	-0.73
1.25	1.22	-0.73	-0.73	0.41	0.09	0.09	0.71	-0.10	-0.10	0.27	0.12	0.12	-0.98	0.59	0.59

*Rounded to two decimal places
**Number of collisions in every timestep: 1st - 0; 2nd - 02; 3rd - 01; 4th - 0; 5th - 02

Test VII: Initial position of the centre of mass: C_o = (0.25, 0.25, 0.25) m; Initial velocity: V_o = (-1.00,-1.50,-1.50) m/s; CR = 0.90; CF = 0.10 (see simulation results in Table VII and Fig. 7).

TABLE VII. Results of the 7th validation test* (SI units).

t**	Input data									Output data					
	V_{ox}	V_{oy}	V_{oz}	C_{ox}	C_{oy}	C_{oz}	C_{1x}	C_{1y}	C_{1z}	C_{fx}	C_{fy}	C_{fz}	V_{fx}	V_{fy}	V_{fz}
0.25	-1.00	-1.50	-1.50	0.25	0.25	0.25	0.00	-0.12	-0.12	0.02	0.13	0.13	0.73	1.09	1.09
0.50	0.73	1.09	1.09	0.02	0.13	0.13	0.20	0.40	0.40	0.20	0.40	0.40	0.73	1.09	1.09
0.75	0.73	1.09	1.09	0.20	0.40	0.40	0.38	0.68	0.68	0.38	0.32	0.32	0.59	-0.89	-0.89
1.00	0.59	-0.89	-0.89	0.38	0.32	0.32	0.53	0.10	0.10	0.45	0.10	0.10	-0.53	-0.80	-0.80
1.25	-0.53	-0.80	-0.80	0.45	0.10	0.10	0.32	-0.10	-0.10	0.32	0.11	0.11	-0.43	0.65	0.65

*Rounded to two decimal places

**Number of collisions in every timestep: 1st - 02; 2nd - 0; 3rd - 01; 4th - 01; 5th - 01

Test VIII: Initial position of the centre of mass: C_o= (0.01, 0.25, 0.25) m; Initial velocity: V_o = (1.50,1.50,0.00) m/s; CR = 0.80; CF = 0.20 (see simulation results in Table VIII and Fig. 8).

TABLE VIII. Results of the 8th validation test* (SI units).

t**	Input data									Output data					
	V_{ox}	V_{oy}	V_{oz}	C_{ox}	C_{oy}	C_{oz}	C_{1x}	C_{1y}	C_{1z}	C_{fx}	C_{fy}	C_{fz}	V_{fx}	V_{fy}	V_{fz}
0.25	1.50	1.50	0.00	0.01	0.25	0.25	0.39	0.62	0.25	0.39	0.38	0.25	1.20	-1.20	0.00
0.50	1.20	-1.20	0.00	0.39	0.38	0.25	0.69	0.08	0.25	0.33	0.08	0.25	-0.96	-0.96	0.00
0.75	-0.96	-0.96	0.00	0.33	0.08	0.25	0.09	-0.16	0.25	0.09	0.14	0.25	-0.77	0.77	0.00
1.00	-0.77	0.77	0.00	0.09	0.14	0.25	-0.10	0.34	0.25	0.10	0.34	0.25	0.61	0.61	0.00
1.25	0.61	0.61	0.00	0.10	0.34	0.25	0.25	0.49	0.25	0.25	0.49	0.25	0.61	0.61	0.00

*Rounded to two decimal places

**Number of collisions in every timestep: 1st - 01; 2nd - 01; 3rd - 01; 4th - 01; 5th - 0

Test IX: Initial position of the centre of mass: C_o = (0.01, 0.01, 0.49) m; Initial velocity: V_o = (1.50, 1.50, 1.00) m/s; CR = 0.85; CF = 0.15 (see simulation results in Table IX and Fig. 9).

TABLE IX. Results of the 9th validation test* (SI units).

t**	Input data									Output data					
	V_{ox}	V_{ov}	V_{oz}	C_{ox}	C_{ov}	C_{oz}	C_{1x}	C_{1v}	C_{1z}	C_{fx}	C_{fv}	C_{fz}	V_{fx}	V_{fv}	V_{fz}
0.25	1.50	1.50	1.00	0.01	0.01	0.49	0.39	0.39	0.74	0.39	0.39	0.28	1.27	1.27	-0.85
0.50	1.27	1.27	-0.85	0.39	0.39	0.28	0.70	0.70	0.07	0.31	0.31	0.07	-0.92	-0.92	-0.61
0.75	-0.92	-0.92	-0.61	0.31	0.31	0.07	0.08	0.08	-0.09	0.08	0.08	0.09	-0.78	-0.78	0.52
1.00	-0.78	-0.78	0.52	0.08	0.08	0.09	-0.12	-0.12	0.22	0.12	0.12	0.22	0.57	0.57	0.38
1.25	0.57	0.57	0.38	0.12	0.12	0.22	0.26	0.26	0.32	0.26	0.26	0.32	0.57	0.57	0.38

*Rounded to two decimal places

**Number of collisions in every timestep: 1st - 01; 2nd - 01; 3rd - 01; 4th - 01; 5th - 0

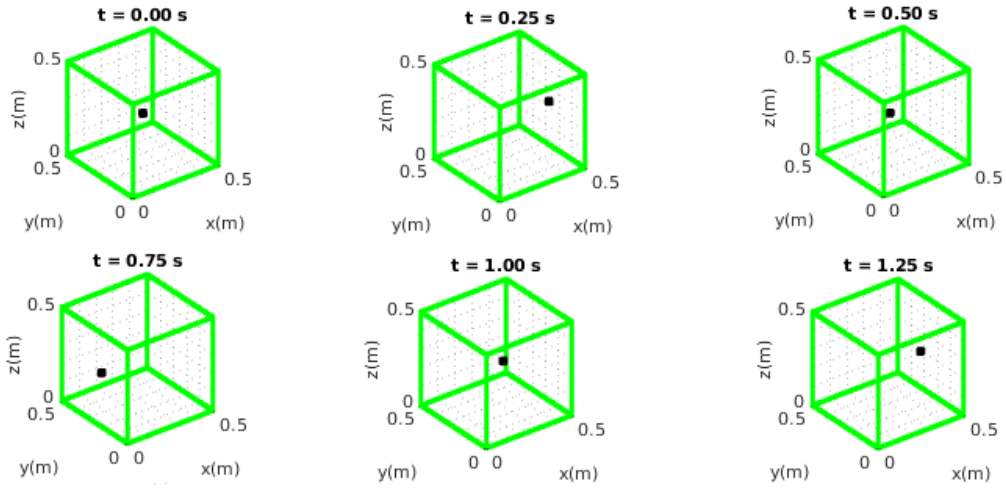

Figure 1. Positions of the centre of mass of the particle at the 1st validation test.

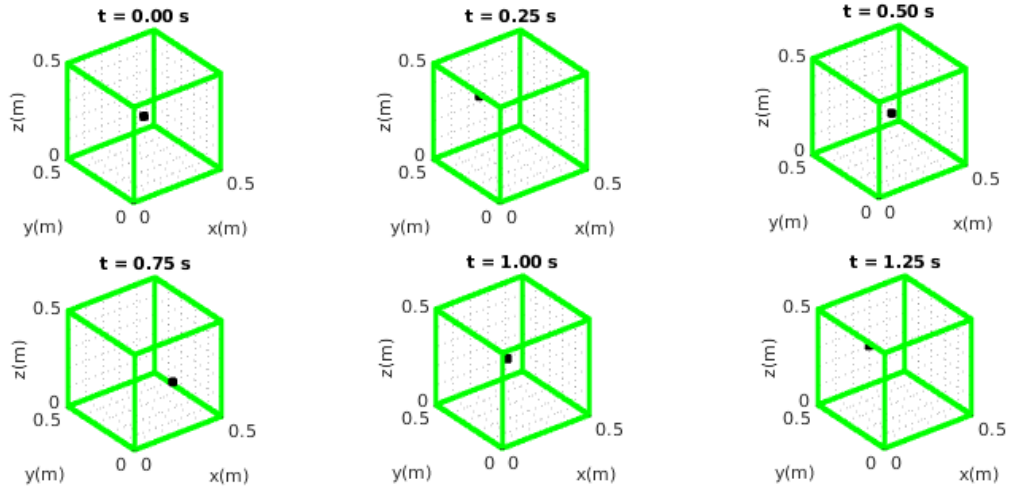

Figure 2. Positions of the centre of mass of the particle at the 2nd validation test.

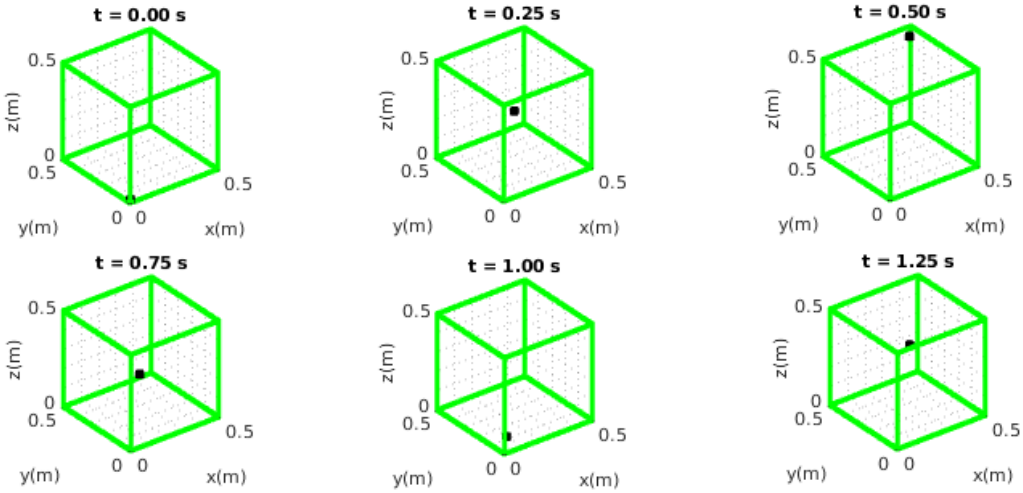

Figure 3. Positions of the centre of mass of the particle at the 3rd validation test.

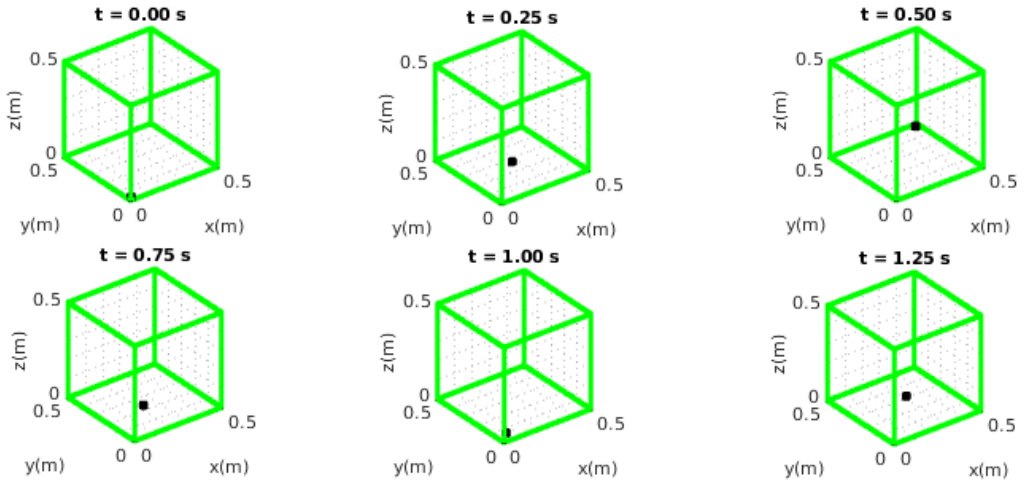

Figure 4. Positions of the centre of mass of the particle at the 4th validation test.

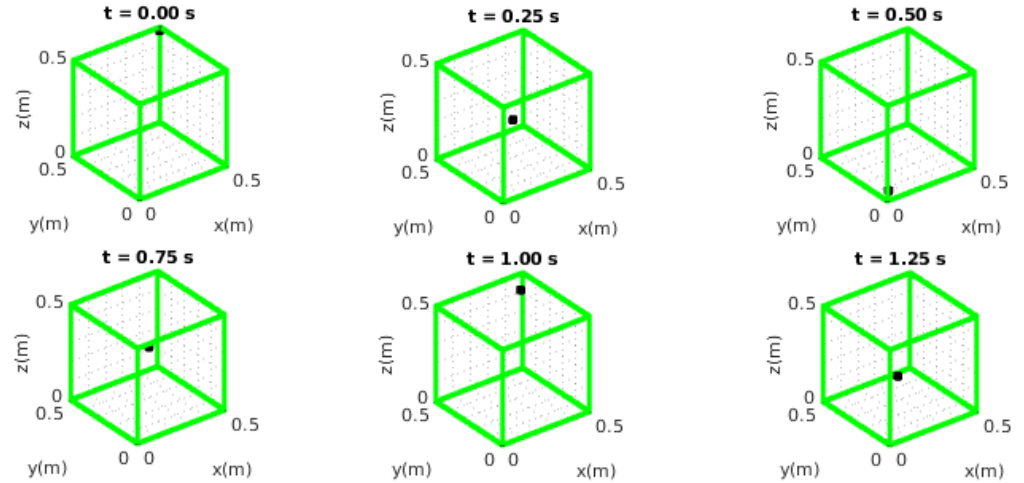

Figure 5. Positions of the centre of mass of the particle at the 5th validation test.

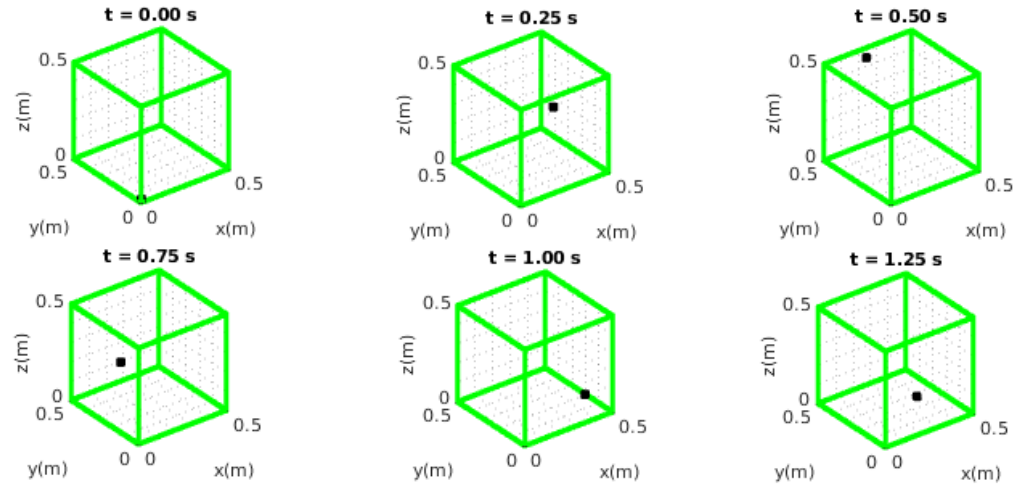

Figure 6. Positions of the centre of mass of the particle at the 6th validation test.

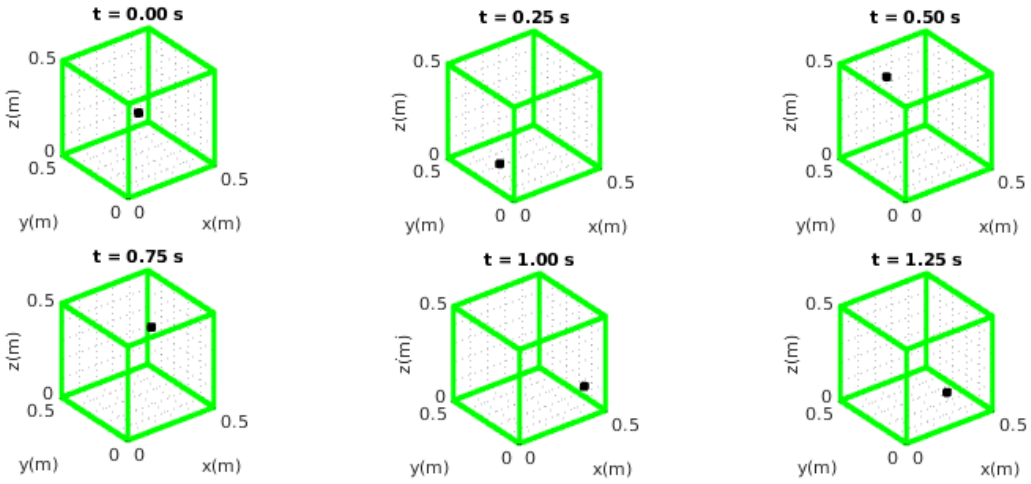

Figure 7. Positions of the centre of mass of the particle at the 7th validation test.

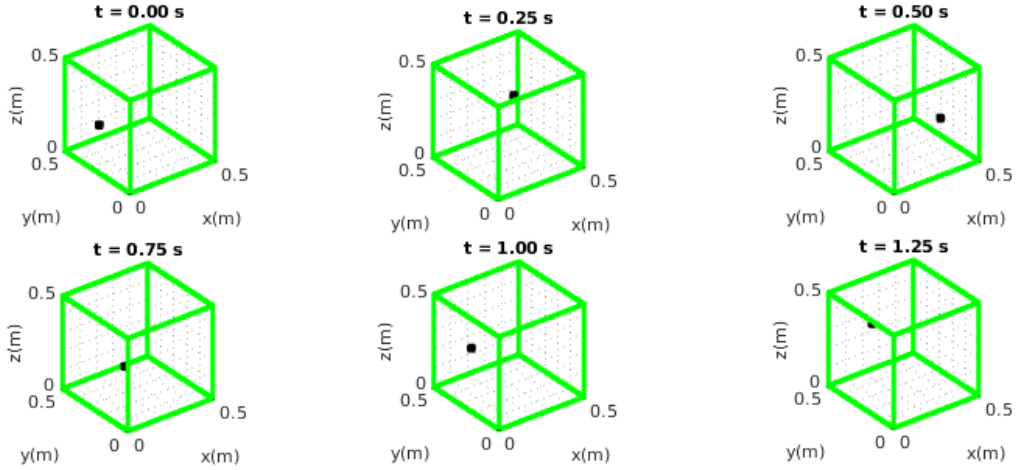

Figure 8. Positions of the centre of mass of the particle at the 8th validation test.

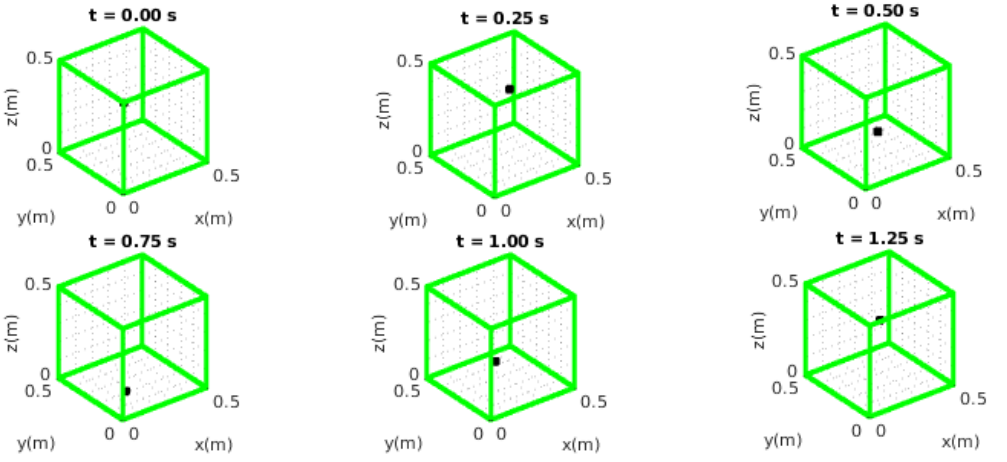

Figure 9. Positions of the centre of mass of the particle at the 9th validation test.

3. Cases Studies

3.1 Still Fluid Inside a Reservoir Open to the Atmosphere

This hydrostatics problem consists of a reservoir open to the atmosphere, filled with a Newtonian, incompressible, uniform and isothermal liquid. The dimensions of the tank are 1.0 m × 1.0 m × 1.0 m. The water particles inside the reservoir are at 20° C and at sea level ($\rho = 1.00 \times 10^3$ kg/m^3, $\nu = 1.00 \times 10^{-6}$ m^2/s). 25 particles per side of the tank (15,625 in total) were used in the discretisation of the fluid.

The modified pressure concept [6] has been used (Eq.(1)) and the physical reflective boundary conditions ensuring the non-motion of the particles and the obedience to the continuum laws.

$$P_{\text{mod}} = (P - P_0) - \rho \text{g}(\text{H} - z) \tag{1}$$

Taking into account that $(P - P_0)$ is the pressure exerted by the fluid column on the particle with vertical coordinate z, the modified pressure is zero to each particle in the domain.

The SPH approximations to the physical laws of conservation of mass and momentum have been employed in the problem solving, Eqs. (2)-(3).

$$\frac{\text{d}\rho_a}{\text{dt}} = \sum_{b=1}^{n} m_b \left(\mathbf{v}_a - \mathbf{v}_b\right).\nabla W(\mathbf{X}_a - \mathbf{X}_b, h) \tag{2}$$

$$\begin{aligned} \frac{\text{d}\mathbf{v}_a}{\text{dt}} = \frac{1}{\rho_a} \sum_{b=1}^{n} m_b \left(P_{\text{mod(b)}} - P_{\text{mod(a)}}\right) \nabla W\left(X_a - X_b, h\right) + \\ + 2\upsilon_a \sum_{b=1}^{n} \frac{m_b}{\rho_b} \mathbf{v}_{ab} \frac{(X_a - X_b)}{\left|X_a - X_b\right|^2}.\nabla W\left(X_a - X_b, h\right) \end{aligned} \tag{3}$$

where $\mathbf{v}_{ab} = \mathbf{v}_a - \mathbf{v}_b$.

Equation (3) is the SPH modified formulation for the momentum conservation equation obtained through application of the concept presented in Eq. (1).

Figure 10 shows the hydrostatic and the modified pressure fields acting on the particles (represented by their centres of mass) inside the reservoir.

The coefficients of restitution of kinetic energy (CR) and friction (CF) were 1.0 and 0.0, respectively. The time step employed was 1.00×10^{-4} s.

The initial velocities of the particle were null. After the solution of the mass and momentum conservation equations and updating of the positions of the centres of mass and velocities of the particles, the positions of the particles remained unchanged (regardless of the interpolation function used in the particle method) and the hydrostatic equilibrium was maintained.

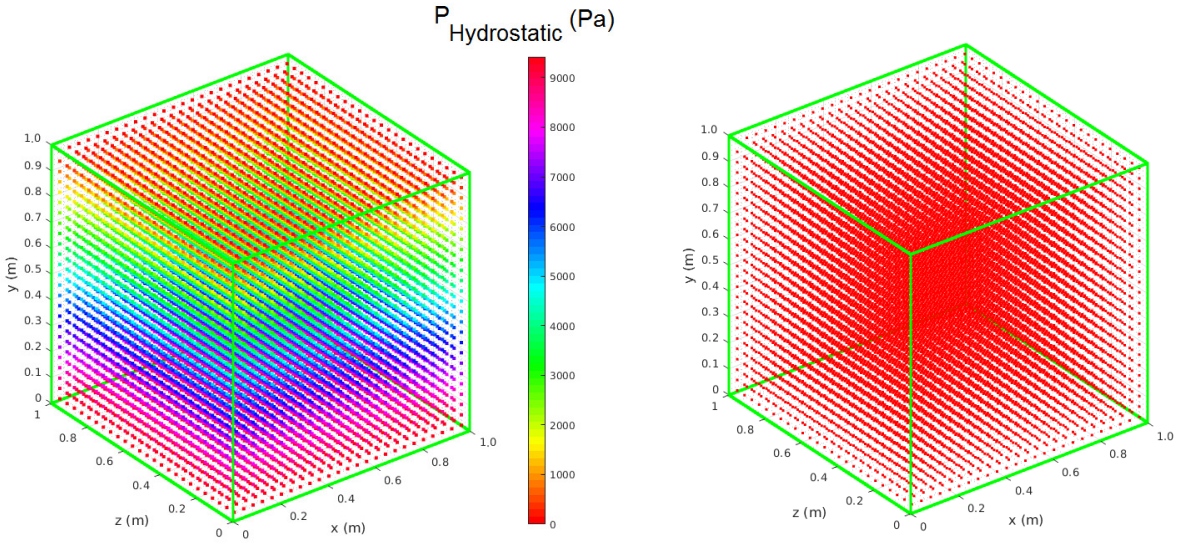

(a) (b)

Figure 10. Pressure acting on the particles inside the reservoir. (a) The hydrostatic pressure field. (b) The modified pressure field (equal to zero). The particles are represented by their centres of mass.

3.2 3-D Dam Break Flow over Dry Bed

The reservoir has length of 0.420 m, height of 0.440 m and depth of 0.228 m. The damned water has a volume with length of 0.114 m, height of 0.228 m, and depth of 0.228 m, discretised by 32,000 particles, with the initial lateral distances between two consecutives centres of mass of 5.70 mm. The water physical properties at 20° C were: $\rho = 1.00 \times 10^3$ kg/m^3 and $\nu = 1.00 \times 10^{-6}$ m^2/s. The water damned was considered incompressible, uniform and isothermal. The standard SPH formulation to the equations of conservation of mass and momentum - Eqs. (2) and (4) - were employed combined with RBC in the boundary treatment (aiming to respect the continuum laws).

$$\frac{\mathrm{d}\rho_a}{\mathrm{dt}} = \sum_{b=1}^{n} m_b \left(\mathbf{v}_a - \mathbf{v}_b\right).\nabla W(\mathbf{X}_a - \mathbf{X}_b, h) \tag{2}$$

$$\begin{aligned} \frac{\mathrm{d}\mathbf{v}_a}{\mathrm{dt}} &= -\sum_{b=1}^{n} m_b \left[\frac{P_a}{{\rho_a}^2} + \frac{P_b}{{\rho_b}^2}\right] \nabla W(\mathbf{X}_a - \mathbf{X}_b, h) + \\ &+ \sum_{b=1}^{n} m_b \left[\frac{2\upsilon_a}{\rho_b} \frac{\left(\mathbf{X}_a - \mathbf{X}_b\right)}{\left|\mathbf{X}_a - \mathbf{X}_b\right|^2}.\nabla W(\mathbf{X}_a - \mathbf{X}_b, h)\right] \left(\mathbf{v}_a - \mathbf{v}_b\right) + \mathbf{g} \end{aligned} \tag{4}$$

The absolute pressure acting on every fluid particle was composed by the sum of two parcels: the hydrostatic and the hydrodynamics (predicted by the Tait equation). The free surface particles were found at the initial time instant and marked. Their absolute pressures were set to zero (Newman boundary conditions). These pressures (on the marked particles) were kept null throughout the numerical simulation.

The simulation timestep was 1.00×10^{-4} s. The temporal integration method employed was 1st order Runge-Kutta integration method (Euler's method).

Density renormalization was performed at every 30 timesteps and the correction of the kernel gradient near the boundaries (where the kernel truncation occurred) was done at each numerical iteration. A support radius varying with time, have been used [7, 8].

In the RBC implementation, the coefficients CR and CF received the values 1.00 and 0.00, respectively. Numerical corrections have been applied in the simulations:

✓ artificial viscosity [7, 8]: to avoid numerical instabilities and the interpenetration between particles (with the coefficients $\alpha_\pi = 0.04$ and $\beta_\pi = 0.00$),

✓ artificial pressure [9] (with the parameters ϵ equal to 0.10 and Δp equal to the initial lateral distance between two consecutives centres of mass) aiming to avoid the tensile instability, related to the particles' interpenetration.

The validation of the results has been done from experimental data and Eulerian finite element method (FEM) results provided by literature [10]. Figure 11 shows the SPH results achieved in this work for the dam breaking flow in some time instants of the simulation.

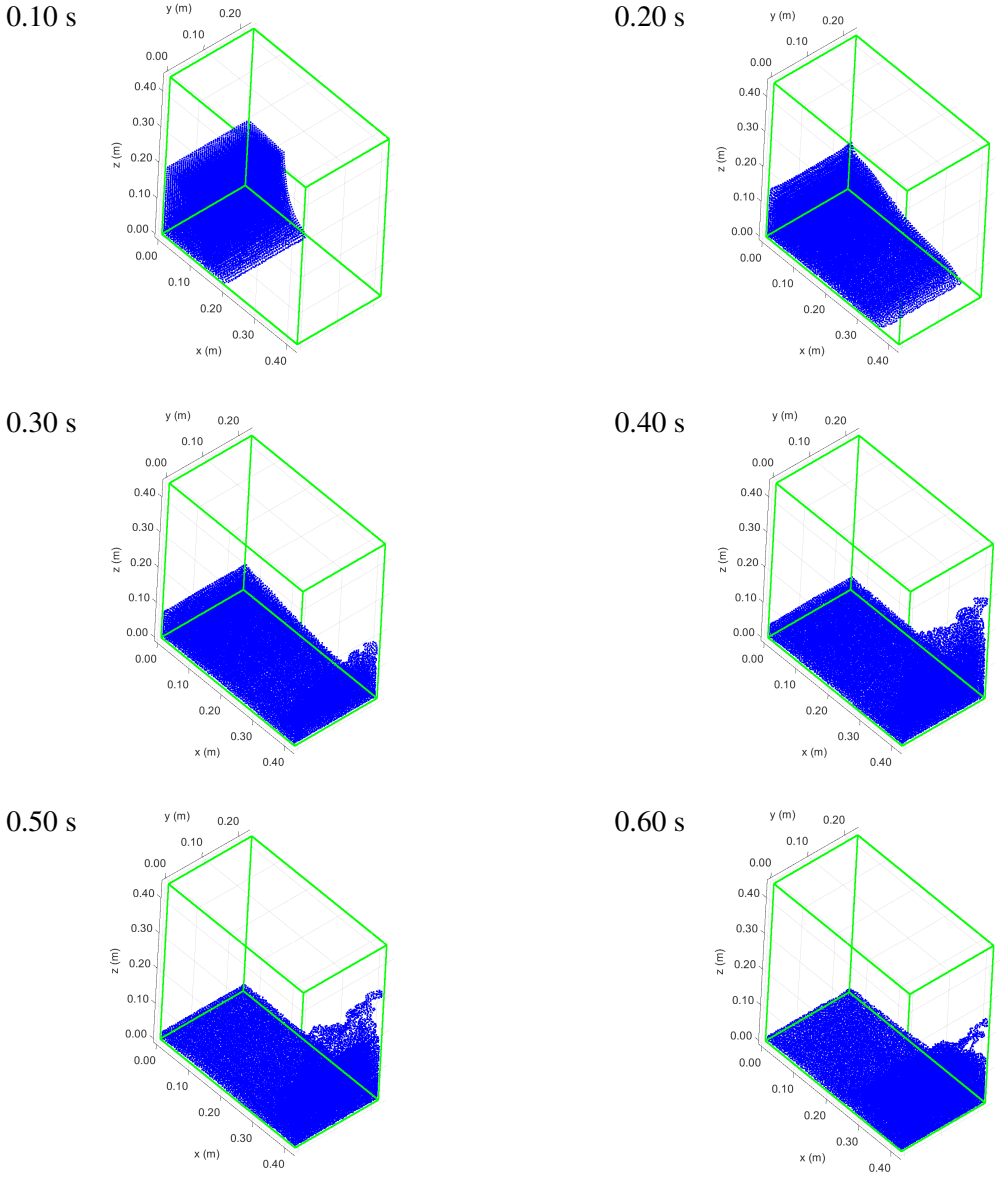

Figure 11. 3-D dam breaking flow evolution (SPH simulation results) until 0.60s.

The evolution of the dam breaking flow (lateral xz cross-section), in some instants of time, is shown in Figs. 12-13. In Figure 12, a comparison between the experimental data [10] and the SPH results is shown. The comparison between FEM results, provided by [10], and the SPH results (achieved in this work) is in Fig. 13.

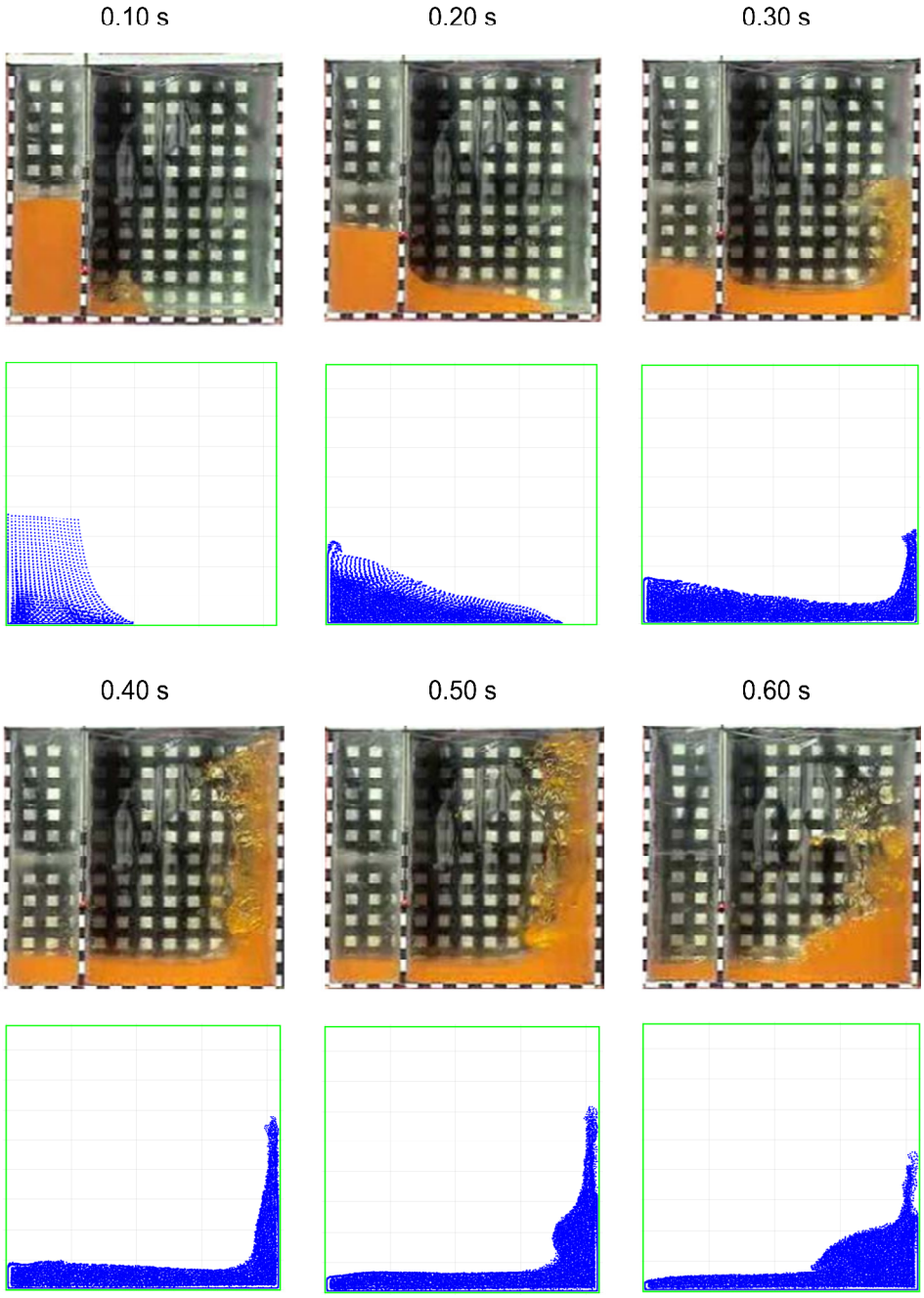

Figure 12. Experimental data [10] and the SPH simulation results (in blue) for different time instants until 0.60 s.

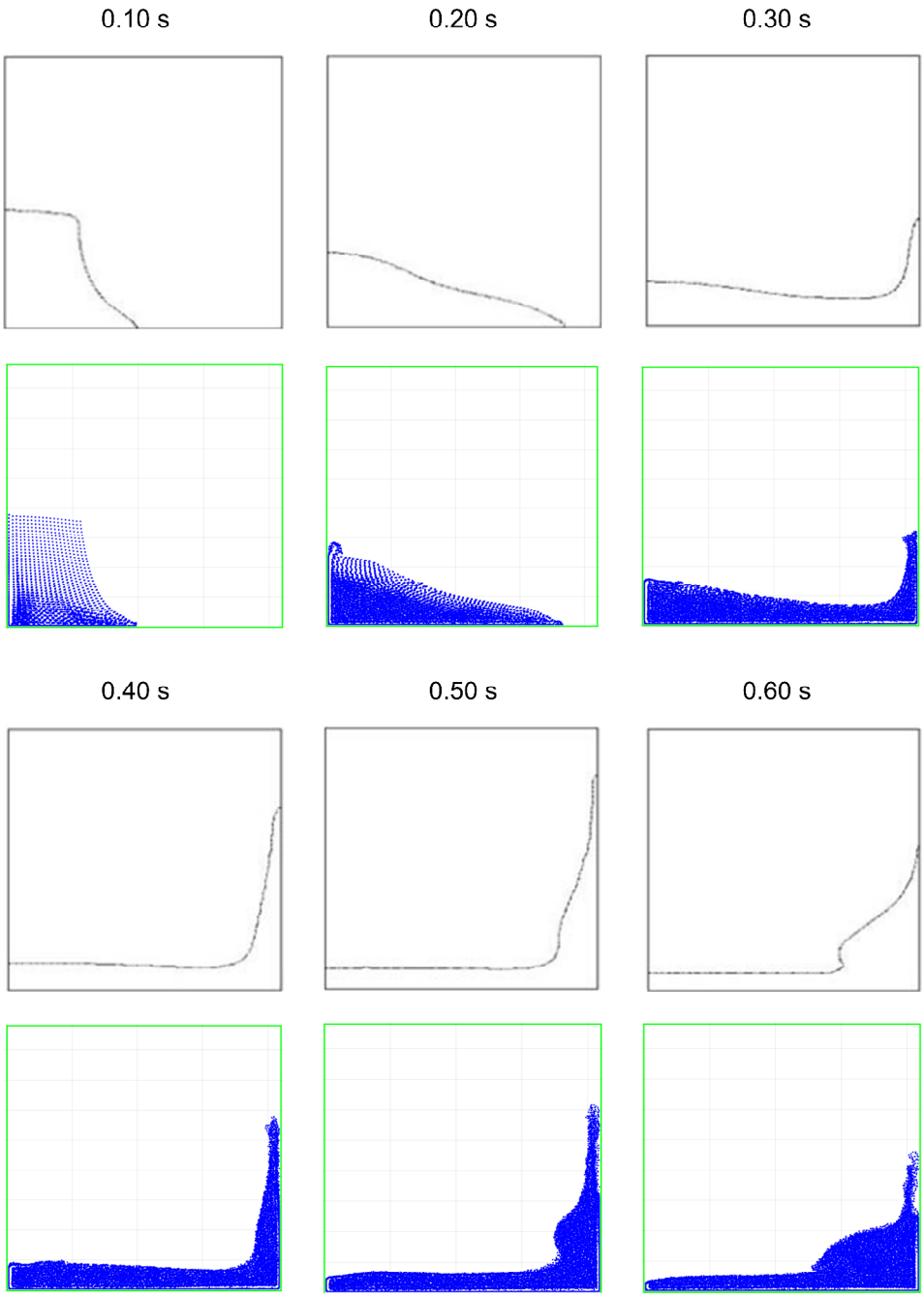

Figure 13. Finite element method (FEM) [10] results (free surface lines) and SPH results for different time instants until 0.60 s.

From the analysis of Figs. 12 and 13, a good agreement, with the experimental data and particularly with the FEM results both provided by [10], has been seen.

4. Conclusions and Future Work

In this work, the implementation of RBC in the 3-D domain has been presented. Validation tests have been performed to verify the results provided by the 3-D collision detection and response algorithm. Simulations of two fluid dynamic cases (hydrostatics and hydrodynamics) have been performed.

In hydrostatics, a Newtonian, incompressible, uniform, and isothermal fluid at rest inside a reservoir has been simulated. The SPH results showed complete agreement with the analytical solution, regardless of the interpolation function employed in the SPH meshfree particle method.

In the hydrodynamics (dam break flow simulation), a good agreement between with the SPH results and the experimental data and Eulerian FEM results, both provided by [10] , has been seen.

In future work, more computational simulations should be performed using different combinations of values for CR and CF, and different parameters in the computational corrections (artificial viscosity and artificial pressure) in order to improve the accuracy of SPH results for the 3D dam break flow.

References

[1] C.A.D. Fraga Filho. On the boundary conditions in Lagrangian Particle Methods and the physical foundation of continuum mechanics, *Continuum Mech. Thermodyn.* 31(2):475–489, 2019 https://doi.org/10.1007/s00161-018-0702-2

[2] C.A.D. Fraga Filho. An algorithmic implementation of physical reflective boundary conditions, *Physics of Fluids* 29, 113602, 2017. https://doi.org/10.1063/1.4997054

[3] M. Ferrand M., D. R. Laurence, B.D. Rogers, D. Violeau and C. Kassiotis. *Unified semi-analytical wall boundary conditions for inviscid, laminar or turbulent flows in the meshless SPH method*. Int. J. Numer. Methods Fluids 71(4): 446–472, 2013. https://doi.org/10.1002/fld.3666

[4] A. Leroy, D. Violeau, M. Ferran and C. Kassiotis. *Unified semi-analytical wall boundary conditions applied to 2-D incompressible SPH*. J. Comput. Phys. 261:106–129, 2014. https://doi.org/10.1016/j.jcp.2013.12.035

[5] A. Mayrhofer, M. Ferrand, C. Kassiotis, D. Violeau and F. Morel. *Unified semi- analytical wall boundary conditions in SPH: analytical extension to 3-D*. Numer. Algorithms 68(1):15–34, 2015. https://doi.org/10.1007/s11075-014-9835-y

[6] C.A.D. Fraga Filho and J.T.A. Chacaltana. Study of Fluid Flows using Smoothed Particle Hydrodynamics: the Modified Pressure Concept Applied to Quiescent Fluid and Dam Breaking. In: *Proceedings of the XXXVI Ibero-Latin American Congress of Computational Methods in Engineering – CILAMCE2015*, Rio de Janeiro (2015). Available at

https://ssl4799.websiteseguro.com/swge5/PROCEEDINGS/PDF/CILAMCE2015-0071.pdf, accessed on May 12, 2019.

[7] C.A.D. Fraga Filho, *Smoothed Particle Hydrodynamics: Fundamentals and Basic Applications in Continuum Mechanics*. Springer Nature, Switzerland, 2019.

[8] G.R. Liu and M.B. Liu. *Smoothed Particle Hydrodynamics: a Meshfree Particle Method*. World Scientific, Singapore, 2003.

[9] J.J. Monaghan, *SPH without tensile instability,* J. Comput. Phys. 159:290–311, 2000. https://doi.org/10.1006/jcph.2000.6439

[10] M.A. Cruchaga, D.J. Celentano and T.E. Tezduyar. *Collapse of a liquid column: numerical simulation and experimental validation*, Comput. Mech. 39(4): 453–476, 2007. https://doi.org/10.1007/s00466-006-0043-z